Contrib Mineral Petrol (2001) 140: 720–733
DOI 10.1007/s004100000216

J. B. Dawson · P. G. Hill · P. D. Kinny

Mineral chemistry of a zircon-bearing, composite, veined and metasomatised upper-mantle peridotite xenolith from kimberlite

Received: 15 May 2000 / Accepted: 12 October 2000 / Published online: 7 February 2001

Abstract Zircon-bearing veins in a harzburgite xenolith from kimberlite have imposed Ca-metasomatism on the harzburgite wall rock, in addition to adding K, Fe, Ti and OH. The zircon, previously dated to have an age similar to that of the xenolith-hosting kimberlite, shows higher Y, Nb, Ba, REE, Th and U contents than other mantle-derived zircons. Peripheral alteration of the zircon to baddeleyite and zirconolite, and alteration of vein ilmenite to perovskite suggest reaction with an evolving carbonatitic kimberlite melt. The high Cr_2O_3 content (0.77 wt%) of the zirconolite extends the compositional range of terrestrial zirconolite.

Introduction

It is now widely accepted that melts and fluids migrating from depth within the upper mantle can have widely differing compositions and impose different types of chemical change (metasomatism) on the dominantly peridotitic wall rocks with which they come into contact (e.g., Bailey and Lloyd 1975; Bailey 1982; Kramers et al. 1983; Navon and Stolper 1987; references in Menzies and Hawkesworth 1987). These metasomatic variations are particularly true on a global scale (Dawson 1984) and, even in relatively small geographical areas such as northern Tanzania, xenoliths from different eruptive sites exhibit a range of metasomatic effects (Dawson 1999). The resulting mineralogy reflects hybridisation between the composition of the original mantle rocks (palaeosome) and the types and abundances of the elements introduced during metasomatism. In many xenoliths, because of their small size, there is no obvious metasomatic source, but in a number of xenoliths the metasomatism can be directly linked to planar features (dykes, veins or zones) infilled with phases differing from those in the palaeosome (e.g., Wilshire et al. 1980; Dawson 1987; Harte et al. 1987; Dawson and Smith 1988).

In the specific case of xenoliths from kimberlite, specimens from Kimberley, South Africa have formed the basis of several metasomatism studies (Carswell 1975; Jones et al. 1982; Kramers et al. 1983; Haggerty et al. 1983, 1989; Erlank et al. 1987). Metasomatic phases developed in the peridotites are clinopyroxene, phlogopite, amphibole, serpentine, ilmenite and rutile. These are chemically similar to phases commonly precipitated in visible veins, except that the phases in the peridotites are more magnesian and also contain more Cr, having developed at the expense of former Cr-pyrope and Cr-diopside. More exotic phases are priderite and Ba-Sr-K titanates (lindsleyite, mathiasite and hawthorneite). From these studies, it is apparent that the dominant metasomatic major-element additions are K, Na, Fe and Ti, whilst Ca enhancement is relatively minor. The present paper reports the mineral chemistry of a veined and metasomatised harzburgite xenolith from Kimberley which provides evidence for further metasomatic complexity in that Ca addition is a major feature. Also reported are inferred chemical changes in the vein fluids reflected in the replacement of zircon by baddeleyeite and zirconolite, and of ilmenite by perovskite.

Sample description

The specimen, BD3024, was collected from the kimberlite waste dump at Boshof Road, Kimberley. It is an angular block measuring approximately 8 × 6 × 5 cm (Fig. 1), its longest sides being planar, mica-coated surfaces. The xenolith is a composite, consisting of a peridotite palaeosome injected by mineralogically (and hence chemically) contrasting veins. The palaeosome consists mainly

J. B. Dawson (✉) · P. G. Hill
Department of Geology and Geophysics,
University of Edinburgh, Edinburgh EH9 3JW, UK
E-mail: barry.dawson@glg.ed.ac.uk

P. D. Kinny
School of Applied Geology, Curtin University,
Perth 6845, Australia

Editorial responsibility: I. Parsons

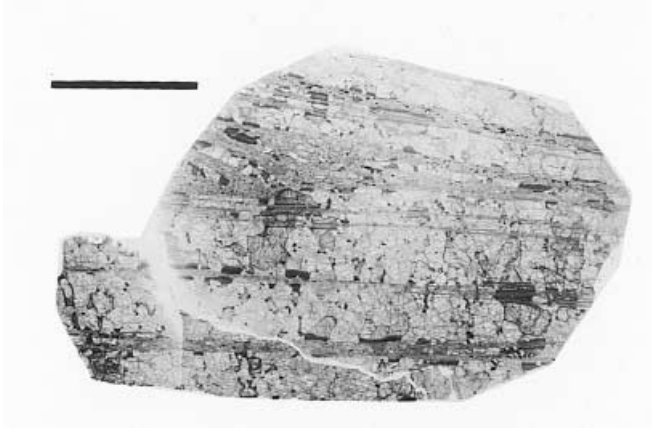

Fig. 1 Thin section of veined harzburgite BD3024, illuminated from the rear. The darker, thin, sub-parallel areas are the veins. *Scale bar* is 20 mm

(~85 vol%) of granular, partially serpentinised olivine up to 8 mm, and subordinate (~4%) enstatite up to 6 mm. Vermicular (fingerprint) spinel (~1%), similar to that reported from other mantle peridotites (Dawson and Smith 1975), is intergrown with some enstatite grains. The block is cut by a series of subparallel planar veins up to 3-mm wide. Most are continuous but others are impersistent, being interrupted by areas of fine-grained (0.1 mm) recrystallised olivine. Where interrupted, there is no offset across the veins, suggesting that the veins are not microshear zones in which the olivine recrystallisation might have been attributed to directed strain.

The veins (Fig. 2) consist of abundant grains of euhedral diopside (400 μm) and phlogopite (1 mm) together with less common ilmenite (up to 500 μm), zircon (200 μm), perovskite (30 μm), apatite (25 μm), and rare globular grains (up to 20 μm) of pyrrhotite and heazlewoodite (a Ni-sulphide), all set in an intergranular matrix of amorphous serpentine and subordinate calcite grains (up to 50 μm). Except for an absence of euhedral olivine, this combination of minerals is similar to that found in kimberlite. The zircon grains are euhedral and up to 200 μm. Some occur as inclusions in mica but most are surrounded by the serpentine/calcite matrix. They have not been seen included in diopside. An earlier geochronological study on the zircons gave a U-Pb age of 84 ± 2 Ma (Kinny and Dawson 1992), which is very close to the 82 ± 2-Ma age for the kimberlite magmatism at Kimberley (Allsopp and Barrett 1975). When examined by backscattered electron (BSE) imaging and cathodoluminescence, only one grain of the fifteen examined was found to have any internal structure, comprising a euhedral core mantled with a single overgrowth (Fig. 3). Externally, some zircons are unaltered but most have been peripherally altered to a phase of composition ZrO_2 which could be either monoclinic baddeleyite or tetragonal ZrO_2. The fine grain size (typically <50 μm) has prevented separation and X-ray diffraction but, for convenience, the phase will be referred to as baddeleyite. Other partial pseudomorphs consist of a core of zircon mantled by coronas of baddeleyite which, in turn, are partly replaced by zirconolite in aggregates up 200 μm (Fig. 4). In some cases, the baddeleyite corona is absent and the zirconolite mantle is directly in contact with zircon (Figs. 3, 4), and in others baddeleyite aggregates (? former zircon) are partly replaced by zirconolite. The zirconolite is not homogeneous, as indicated by slightly different intergrain and intragrain brightness in BSE images which itself reflects chemical variation (see below). The zircon and zirconolite have similar BSE coefficients ($Z = 25.3$ for zircon, and 24.2 for zirconolite), and textural relationships are best revealed by X-ray imaging, particu-

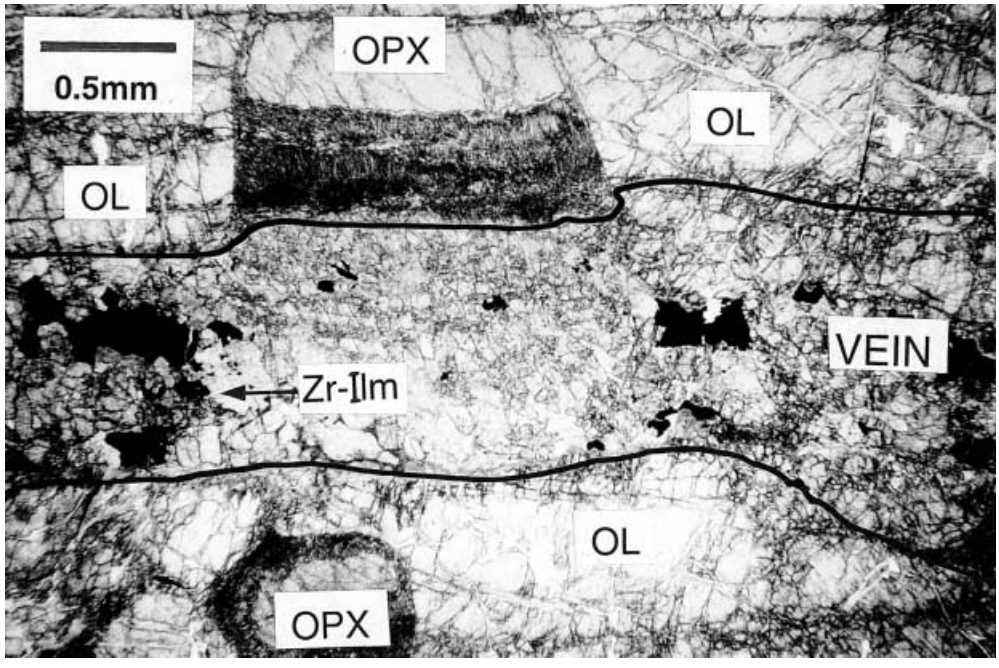

Fig. 2 Photomicrograph of vein in harzburgite (plane-polarised light). The vein/palaeosome contact has been inked in for clarity. Note absence of visible olivine(*OL*)/vein interaction, contrasting with a well developed reaction rim on enstatite (*OPX*). Small enstatite grain in harzburgite palaeosome also has thin reaction corona. *Zr-Ilm* Zircon-ilmenite cluster

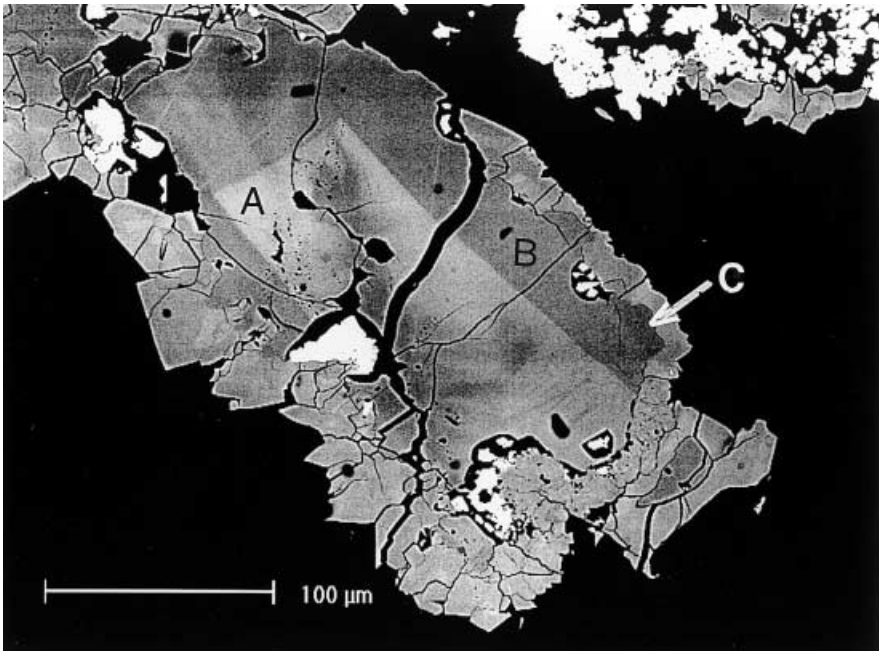

Fig. 3 BSE image of an atypical zoned zircon (most show no internal structure). A homogeneous euhedral core is mantled by a single overgrowth zone. The grain has a thin peripheral rind of replacing zirconolite, not readily discernible in BSEI (however, see Figs. 4 and 5). The very *bright phase* is baddeleyite. Points *A–C* correspond to analyses 2–4 in Table 3

larly for Ca and Ti (Figs. 4, 5). Some zirconolite-mantled grains are partly embedded in ilmenite grains, although separated from the ilmenite by thin films of serpentine and calcite (Fig. 5). A feature of these ilmenite/zircon "intergrowths" is that zirconolite is also present on zircon surfaces which are not embedded in ilmenite (Fig. 5). The ilmenite grains, up to 2 mm, vary in shape from rounded to elongate or cuspate. Like the zircons, many ilmenite grains are unaltered but a small number have suffered peripheral alteration, in these cases to coronas of perovskite and Mg-Cr-Ti spinel (Fig. 6).

Wall-rock alteration

At the contact between the vein and the wall-rock harzburgite, there has been some interaction. Optically, the olivine immediately adjacent to the vein appears to be unaffected, though electron-probe microanalyses (see below) show that it contains more Fe, Mn and Ca than olivine further away from the vein. In contrast, the wall-rock orthopyroxene is visibly altered and has reaction fringes adjacent to the veins. The fringes are intergrowths of fine-grained (<0.01 mm) acicular diopside and richterite oriented normal to the wall rock/vein contact, with intergranular phlogopite, serpentine and tiny (50 μm) grains of apatite and pyrrhotite. Similar reaction fringes occur on enstatite grains within the palaeosome but close to the veins (Fig. 2).

Whole-rock chemistry

The whole-rock analysis of this rock, reported earlier by Dawson (1987), is given here as a background to the phase chemistry: SiO_2 42.51, TiO_2 0.94, Al_2O_3 1.10, Fe_2O_3 2.18, FeO 5.20, MnO 0.12, MgO 39.48, CaO 3.08, Na_2O 0.19, K_2O 0.60, H_2O^+ 3.23, CO_2 0.24, P_2O_5 0.11, SO_3 0.04, sum 99.00 wt%; trace elements (ppm): V 76, Cr 2084, Ni 1924, Cu 42, Zn 49, Rb 27, Sr 95, Y 2, Zr 340, Nb 31, Ba 93, and Pb 5.

Compared with other kimberlite-hosted harzburgites, the rock's enhancement in total Fe, Ti, Ca, Na, K, Rb, Sr, Zr, Ba and Cu reflects their presence in the vein minerals.

Analytical methods

The minerals were analysed by wavelength-dispersive spectroscopy (WDS) on a Camebax Microbeam electron microprobe at the University of Edinburgh. The analytical conditions and standards for most of the phases are given in Dawson and Hill (1998), and additional standards used in the present investigation were Hf and Ta metal and synthetic thorite (substituted for Th metal).

In the case of the high-zirconium phases (zircon, baddeleyite and zirconolite), a slightly different routine was adopted. Because preliminary analyses indicated them to be below detection, Mg and Al were dropped from the programme. Counting times for other elements were 30 s on peaks except for Nb (60 s) and yttrium (90 s). Background counts were made for half the peak times, except for Y, Hf and Th when counts were the same as for peaks. In the presence of high amounts of Zr, and because of peak overlaps, there are problems in the determination of Nb. We measured Nb on its Lα peak which is close to the Zr Lβ6 peak. However, because of the trivial amounts of Nb detected in both zircon and baddeleyite (the phases with the highest Zr contents), enhancement of the Nb Lα counts by slight overlap with the Zr Lβ6 peak appears to be minimal. Hence, we believe the relatively high Nb contents in the zirconolite to be real.

Trace elements in zircon and ilmenite were analysed by secondary ion mass spectrometry on the Cameca ims-4f ion microprobe at the University of Edinburgh. The analytical routine used an $^{16}O^-$ primary beam of 15 kV energy and analysed the positive secondary ions. The energy filtering techniques are those of Zinner and Crozaz (1986). The standard used was glass SRM160. Ion yields were normalised to Si for the zircon analyses, and to Ti for the ilmenite. Absolute contents are within 20%.

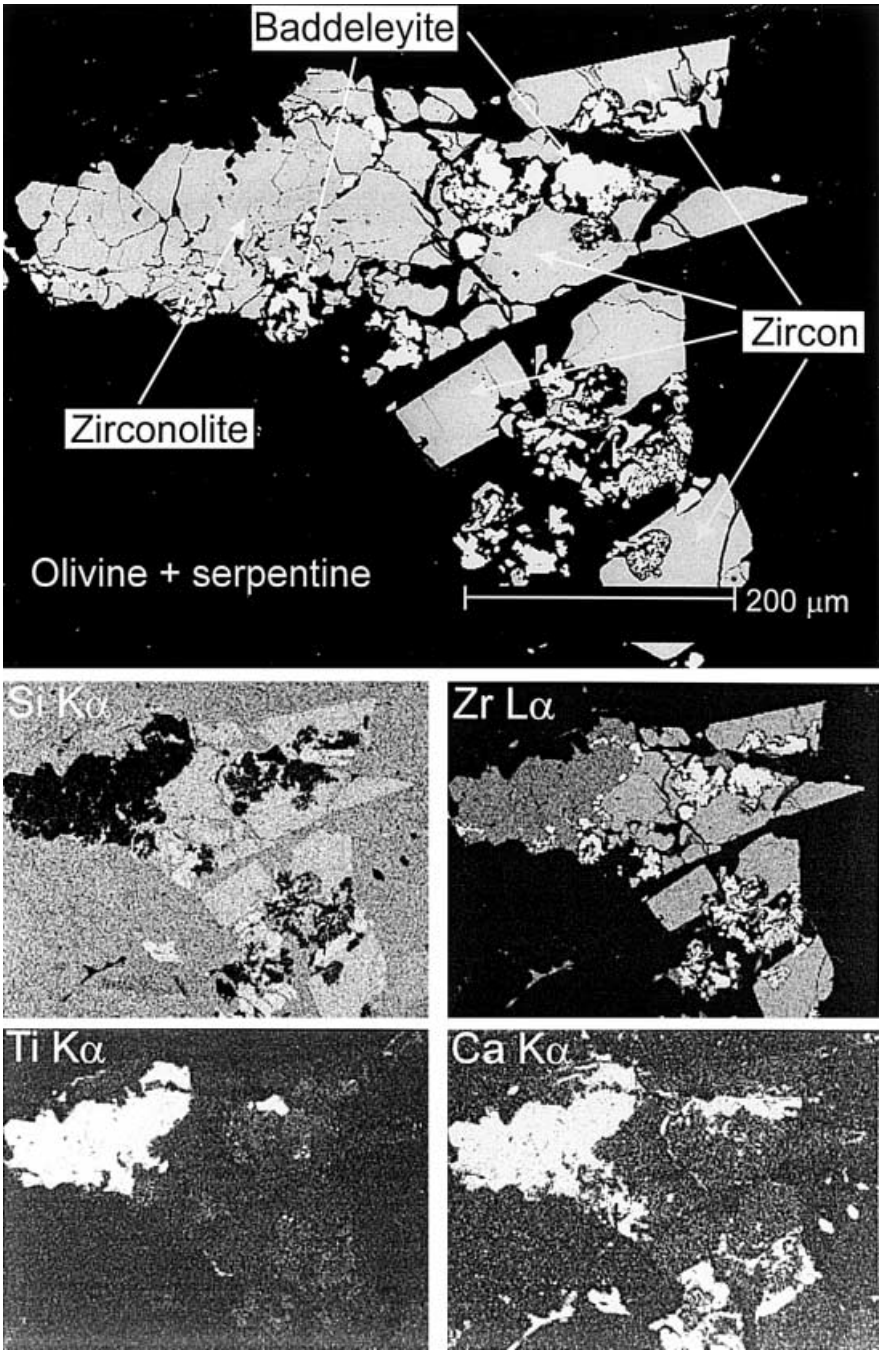

Fig. 4 BSE and X-ray images of partly altered zircon. Whereas the bright baddeleyite is readily seen on the BSE image, zircon and zirconolite are almost indistinguishable but they are readily resolved on the Si, Ca, and Ti X-ray images

Mineral chemistry – phases in the harzburgite palaeosome

Olivine

The olivine is a low-Ca forsterite (Fo_{93}; Table 1, analysis 1) which falls towards the more magnesian end of the range for mantle olivines ($Fo_{88–94}$; Hervig et al. 1986). However, the grain margins immediately adjacent to the veins contain more Fe (Fo_{91}), Mn, and particularly Ca (Table 1, analysis 2). The Ca contents in the grain margins are about five times that of olivine more distant from the veins.

Orthopyroxene

Unaltered orthopyroxene (Table 1, analysis 3) is an enstatite (En_{93}) which, in view of its relatively high Al_2O_3, Cr_2O_3 and CaO contents (2.77, 0.76 and 0.80 wt%, respectively), resembles the orthopyroxene in fertile, rather than barren harzburgites (compare with analyses 4 and 5, Table 1). Adjacent to the veins, the enstatite is converted to a fringe of fine-grained intergrown chromiferous diopside, chromiferous richterite (Table 1, analyses 7, 8) and phlogopite. Compared with the replaced enstatite, the replacing diopside/richterite/

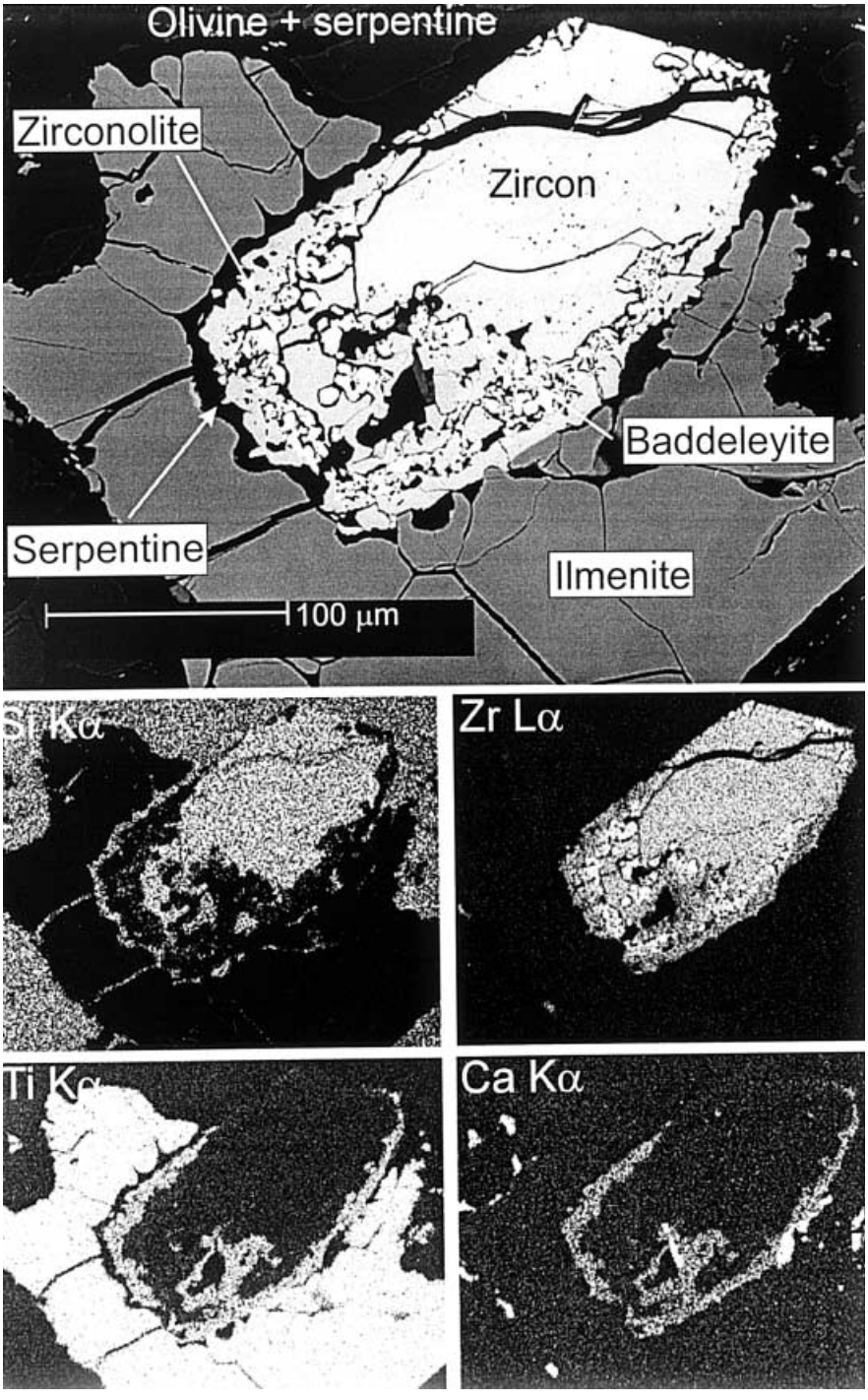

Fig. 5 BSE and X-ray images of an euhedral zircon/baddeleyite/zirconolite composite grain partly embedded in ilmenite. Note the thin band of serpentine separating this grain from the ilmenite, and the occurrence of a partial zirconolite mantle on the end of the zircon not embedded in ilmenite. *Bright spots* on the Ca X-ray image are calcite or apatite

phlogopite combination is much higher in Fe, Ti, Al, Ca, Na and K which must be assumed to have been added from the veins.

Spinel

Smith and Dawson (1975) observed a considerable range in Cr/(Cr + Al) in spinels from mantle peridotites. The relatively low Cr_2O_3 contents in BD3024 spinel (44.9 wt%, Table 1, analysis 6) are more similar to those in spinels from lherzolites or fertile harzburgites, rather than to those in refractory harzburgites in which Cr_2O_3 is generally >60 wt% (e.g., Hervig et al. 1980; Boyd et al. 1993).

Mineral chemistry – phases in the veins

Diopside

The clinopyroxene (Table 2, analysis 1) is a diopside which contains more Ti and Fe but less Cr and Na than

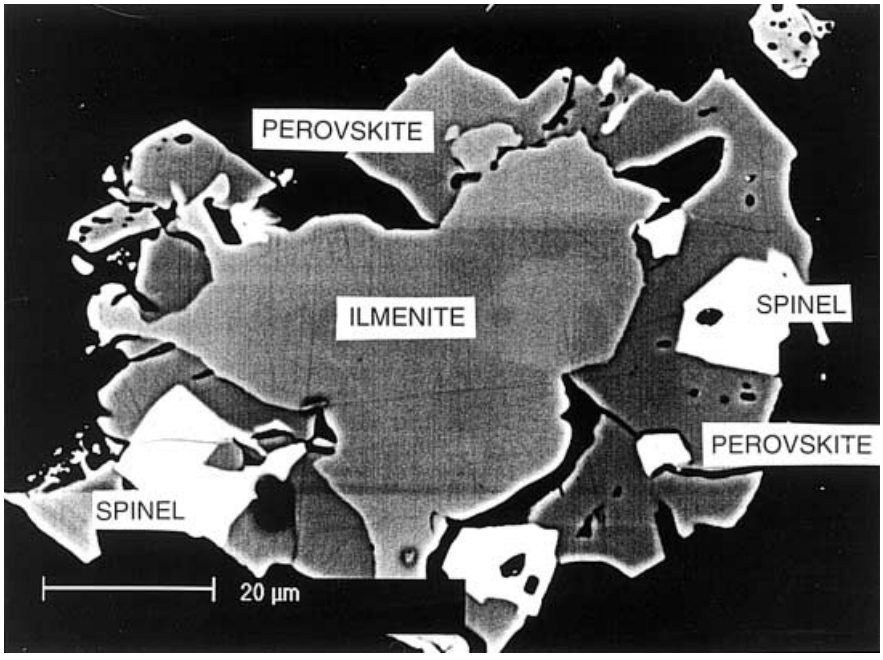

Fig. 6 BSE image of ilmenite with a reaction corona of perovskite and Ti-Cr spinel

Table 1 Analyses of phases in peridotite wall rock. *1* Olivine. *2* Same olivine immediately adjacent to vein. *3* Enstatite. *4* Mean of nine low-Na enstatites in fertile harzburgites (Dawson et al. 1980). *5* Mean of 13 enstatites from barren harzburgites (Dawson et al. 1980). *6* Magnesian fingerprint spinel (Cr/(Cr + Al) 0.53; sum includes 1.62 wt% Fe_2O_3, calculated by stoichiometry). *7* Diopside in fine-grained alteration fringe on enstatite. *8* Richterite intergrown with diopside (analysis 7) in fine-grained alteration fringe on enstatite (total includes 1.74 wt% K_2O, 0.46 wt% F, and –0.20 wt% O ≡ F)

	1	2	3	4	5	6	7	8
SiO_2	40.8	40.3	56.0	57.4	58.5	0.05	54.3	53.5
TiO_2	0.02	0.01	0.01	0.00	0.00	0.04	0.24	0.59
Al_2O_3	0.01	0.01	2.77	2.91	0.96	24.8	0.24	2.39
Cr_2O_3	0.02	0.02	0.76	0.79	0.32	44.9	1.39	1.13
FeO	7.17	8.48	4.68	4.43	4.24	14.0	4.15	3.25
MnO	0.10	0.16	0.13	0.06	0.10	0.31	0.13	0.07
MgO	52.3	50.1	35.3	34.9	35.9	14.2	16.3	22.0
NiO	0.40	0.37	0.10	0.08	0.07	0.07	n.a.	n.a.
CaO	0.01	0.10	0.80	0.83	0.23	0.00	22.3	7.12
Na_2O	0.00	0.00	0.01	0.03	0.02	0.00	1.15	4.83
Total	100.83	99.55	100.56	100.47	100.35	99.99	100.20	96.88
mg [a]	0.93	0.91	0.93			0.64		

[a] $Mg/(Mg + Fe^2)$

the diopside in the metasomatic fringe on the palaeosome enstatite. Although it contains significant Cr_2O_3, it shows lower contents than the Cr-diopsides in upper-mantle lherzolites which also contain more Al_2O_3 (around 2.5 wt%) and less FeO (~2.0 wt%; Stephens and Dawson 1977). Its low Al_2O_3 content (0.26 wt%) makes it similar to MARID suite diopsides, which are mainly in the range 0.2 to 1.5 wt% (Dawson and Smith 1977; Waters 1987; Waters et al. 1989) or the least aluminous of the clinopyroxenes in micaceous kimberlites in which Al_2O_3 contents range between 0 and 1.5 wt% (Dawson et al. 1977; Mitchell 1995).

Mica

The vein mica (Table 2, analysis 2) is a titaniferous (2.17 wt% TiO_2) phlogopite characterised, like the diopside, by low contents of Cr_2O_3 (0.14 wt%) and Al_2O_3 (10.8 wt%), all of which serve to set it apart from primary and secondary micas in peridotite xenoliths (Delaney et al. 1980). Although in many respects it resembles micas in MARID xenoliths, which are likewise low in Al_2O_3 (< 11 wt%; Dawson and Smith 1977), the mica is also similar to the Type II groundmass micas in micaceous kimberlites (Smith et al. 1978), particularly in its high BaO content (0.58 wt%).

Zircon

In the zircon (Table 3, analyses 1–4), the only significant minor element is Hf and its content of 1.24 wt% HfO_2 gives a Zr/Hf ratio (46.1) within the range found for kimberlite zircon megacrysts (range 16 to 79, and mainly <50; cf. review by Mitchell 1986). Zirconium contents are constant within and between grains, and hafnium concentration variation is small (range 1.11 to 1.37 wt%). In the one zoned grain found, differences in brightness in BSE imaging (Fig. 3) can be attributed to higher contents of Th, Y and Ce in the brighter areas (compare analyses 2–4, Table 3). As there is a positive correlation between Th and U in the zircons (Kinny and Dawson 1992), variations in trace amounts of U may also contribute to differences in brightness. Trace-element analyses of 17 spots in six zircon grains are given in Table 4, together with comparative data for zircon megacrysts from on-craton southern African kimberlites and for a single zircon in a MARID xenolith from the Kamfersdam kimberlite, Kimberley (Belousova et al. (1998) also give

Table 2 Compositions of phases in veins. *1* Diopside. *2* Phlogopite (mean of six analyses; total includes 0.22 wt% BaO, 0.58 wt% F, and –0.26 wt% O ≡ F). *3* Intergranular serpentine. *4* Calcite (total includes 0.31 wt% SrO). *5* Apatite (total includes 40.3 wt% P_2O_5, 0.27 wt% La_2O_3, 0.53 wt% Ce_2O_3, and 0.21 wt% Nd_2O_3; SrO below detection limits). *6* Perovskite grain (80 μm) in serpentine matrix (total includes 0.46 wt% Nb_2O_5, 0.16 wt% La_2O_3, 0.40 wt% Ce_2O_3, and 0.16 wt% Nd_2O_3). *7* Mean of three perovskites in perovskite/spinel replacement rim round ilmenite (Fig. 6; total includes 0.41 wt% Nb_2O_5, 0.13 wt%La_2O_3, 0.36 wt% Ce_2O_3, and 0.14 wt% Nd_2O_3). *8* Magnesian ilmenite (total includes 0.17 wt% Nb_2O_5, 0.23 wt% NiO, and 0.01 wt% ZnO). *9* Spinel in perovskite/spinel replacement rim round ilmenite (Fig. 6; total includes 0.48 wt% NiO and 0.08 wt% ZnO). *10* Groundmass spinel, surrounded by phlogopite (total includes 0.34 wt% NiO and 0.09 wt% ZnO)

	1	2	3	4	5	6	7	8	9	10
SiO_2	53.7	40.5	40.3	0.00	0.18	0.11	0.06	0.01	0.08	0.06
TiO_2	0.52	2.17	0.10	n.a.	n.a.	56.5	57.0	56.1	20.6	21.4
ZrO_2	n.a.	n.a.	n.a.	n.a.	n.a.	0.65	0.45	0.29	0.21	0.07
Cr_2O_3	0.26	0.14	0.00	n.a.	n.a.	n.a.	n.a.	1.38	7.17	3.98
Al_2O_3	0.23	10.8	0.25	0.00	0.00	0.05	0.04	0.13	1.22	0.89
FeO	4.77	5.47	6.82	0.16	0.27[a]	1.08	1.05	29.2	57.3	61.8
MnO	0.14	0.04	0.19	0.11	0.02	0.00	0.00	0.50	0.59	0.77
MgO	16.4	24.0	36.5	0.29	0.31	0.05	0.05	12.7	9.48	7.91
CaO	22.9	0.00	0.00	56.4	52.9	39.5	38.9	0.29	0.36	0.06
Na_2O	0.58	0.53	0.00	0.00	0.49	0.79	0.78	0.00	0.00	0.00
K_2O	0.03	9.73	0.00	0.00	n.a.	0.00	0.00	0.00	0.00	0.02
Total	99.51	93.99	84.26	57.27	97.41	99.91	99.37	99.93	97.57	97.55

[a] Total iron as Fe_2O_3, otherwise all iron as FeO
n.a. Not analysed

further data for Russian and off-craton occurrences). Unlike Zr and Hf, the trace-element contents may vary both within and between grains. For example, in grain B1 contents of Nb, Ba and La vary fourfold between different spots, whereas Sr, the other REE, Th and U vary by a factor of only 2. Y and Pb contents are reasonably constant within this grain. Compared with the other mantle-derived zircons (Table 4), those in BD3024 are extremely enhanced in all the trace elements listed, the only similar concentrations being for Pb in a MARID zircon. The REE enhancements, especially for the LREE, are well seen on a chondrite-normalised REE plot (Fig. 7) in which there is a positive Ce anomaly which appears to be typical of many zircons (e.g., Belousova et al. 1998; Hoskin and Ireland 2000). However, the flatness of the pattern for the MREE and HREE (Gd to Lu) is in con-

Table 3 Analyses of zircon, baddeleyite and zirconolite in BD3024, and comparative analyses of zirconolite in other ultramafic rocks. *1* Zircon (mean of eight analyses; Zr/Hf 46.1). *2* Zircon, bright core in BSE image, point A in Fig. 3. *3* Zircon, dark overgrowth, point B in Fig. 3. *4* Zircon, darkest rim, point C in Fig. 3. *5* Baddeleyite (mean of 12 analyses). *6–7* Baddeleyite, two most extreme compositions with respect to Zr and Ti (Zr/Hf 50.9 and 52.0). *8* Zirconolite (mean of 15 analyses; Zr/Hf 43.8). *9–10* Zirconolite, the two most extreme compositions with respect to Zr, Ti and Ca. Analysis 9 is of relatively bright zirconolite (in BSE imaging), reflecting higher Z. *11* From Zircon/ilmenite intergrowth in kimberlite, Kimberley, South Africa (Raber and Haggerty 1979). *12* From Ultramafic adcumulate, Laouni ultrabasic complex, Algeria (Lorand and Cottin 1987). *13* From Olivine-rich mesocumulate, Rhum layered complex, Scotland (Fowler and Williams 1986). *n.d.* Below detection limit at 2σ level; *n.a.* Not analysed (see text); – Not reported

	1	2	3	4	5	6	7	8	9	10	11	12	13
Nb_2O_5	0.02	0.13	n.d.	n.d.	0.04	n.d.	n.d.	0.25	0.23	0.33	–	0.22	0.25
Ta_2O_5	0.03	0.02	0.13	n.d.	0.08	0.16	0.08	0.07	0.03	0.05	–	–	–
SiO_2	32.8	32.8	32.8	32.6	0.01	n.d.	0.13	0.21	0.09	0.19	–	–	0.00
TiO_2	0.13	0.15	0.08	0.13	3.83	5.36	2.75	36.2	34.8	37.7	40.48	35.67	35.73
ZrO_2	65.9	65.6	65.9	65.6	96.6	94.3	97.0	44.4	46.4	42.5	41.91	43.58	44.18
HfO_2	1.24	1.19	1.20	1.37	1.68	1.62	1.63	0.88	0.92	0.93	–	0.34	0.57
ThO_2	0.16	0.48	0.10	0.05	0.04	n.d.	0.09	0.04	0.05	0.04	–	0.41	0.59
Cr_2O_3	0.03	0.04	0.03	0.03	0.05	0.08	0.04	0.77	0.80	0.77	0.09	0.05	0.05
Al_2O_3	n.a.	n.a.	n.a.	n.a.	n.a.	n.a.	n.a.	n.a.	n.a.	n.a.	0.23	0.59	0.50
Y_2O_3	0.10	0.15	0.13	0.05	0.05	n.d.	n.d.	0.04	0.04	n.d.	–	2.50	2.45
La_2O_3	0.00	n.d.	n.d.	n.d.	n.d.	n.d.	n.d.	0.03	0.03	0.02	–	0.02	0.01
Ce_2O_3	0.07	0.12	0.07	0.04	0.08	0.11	0.06	0.29	0.35	0.32	–	0.18	0.13
Pr_2O_3	n.d.	n.d.	n.d.	n.d.	n.d.	n.d.	n.d.	n.d.	n.d.	n.d.	–	0.15	0.13
Nd_2O_3	n.d.	n.d.	n.d.	n.d.	0.04	n.d.	n.d.	0.11	0.09	0.04	–	0.17	0.25
Sm_2O_3	n.d.	n.d.	n.d.	n.d.	n.d.	n.d.	n.d.	n.d.	n.d.	n.d.	–	–	–
FeO	0.13	0.13	0.13	0.15	0.50	0.62	0.45	4.99	5.43	4.36	5.15	4.85	4.87
MnO	0.02	0.02	0.03	n.d.	0.02	0.04	0.03	0.10	0.13	0.08	0.11	–	0.16
MgO	n.a.	n.a.	n.a.	n.a.	n.a.	n.a.	n.a.	n.a.	n.a.	n.a.	0.49	0.19	0.20
CaO	0.06	0.06	0.07	0.03	0.23	0.58	0.20	11.3	10.6	12.1	11.10	10.67	11.15
Total	100.71	99.89	99.66	99.92	103.24	102.87	102.46	99.68	99.99	99.43	99.56	99.59	101.28

trast to the sloping pattern for the other zircons, and serves to emphasise the relative enrichment in the LREE. Further, in its absence of a negative Eu anomaly, the BD3024 zircon pattern is similar to patterns in zircon from the Mud Tank carbonatite (Australia) and the Jwaneng kimberlite (Botswana) but it differs from zircons in more siliceous igneous rocks and in high-grade metamorphics (Hoskin and Ireland 2000). The values given here for Th and U (averages 1,028 and 324 ppm, respectively) are very similar to those found on the A.N.U. SHRIMP, reported in our earlier geochronology study (Kinny and Dawson 1992). These contents are considerably higher than in the other mantle-derived zircons listed in Table 4, and also higher than values of 359–659 ppm U and 254–557 ppm Th (Th/U 0.67–0.85) in a zircon included in diamond from Zaire (Kinny and Meyer 1994), and than the values of 48 to 131 ppm U reported in zircon megacrysts from the Mbuji Mayi kimberlite, Democratic Republic of the Congo (Schärer et al. 1997). The relatively high contents of Th in the BD3024 zircons, and resulting high Th/U ratios (average 3.17) are particularly distinctive. Values of 14–1,066 ppm U in zircons from three MARID xenoliths from kimberlite intrusions in the Kimberley area (Konzett et al. 1998) match the U contents in BD3024 zircons, but the Th contents (4–458 ppm) and Th/U ratios (0.2–0.86) are significantly lower.

Baddeleyite

The main minor oxides in the baddeleyite are TiO_2 (varying from 2.7 to 5.4 wt%), HfO_2 (1.63%) and iron (equivalent to ~0.4 to 0.6 wt% FeO; Table 3, analyses 5 and 6). Zr and Ti contents vary inversely. The three minor elements appear to be ubiquitous in baddeleyites in general (Heaman and Le Cheminant 1993), though analyses in the literature indicate that they occur in quite variable amounts. For example, baddeleyite from the Benfontein kimberlite contains low TiO_2 (up to 0.8%), up to 1.31% FeO, and the Zr/Hf ratio is 49 (Scatena-Wachel and Jones 1984), whereas baddeleyite formed by subsolidus reaction between zircon and ilmenite in composite grains from the Monastery and Mothae kimberlites contains higher TiO_2 (up to 6.10 wt%; Raber and Haggerty 1979). The elemental Zr/Hf ratio of 51 to 52 in the BD3024 baddeleyite compares with 46.1 for the parental zircon, suggesting a small amount of fractionation of Hf from Zr during the alteration process.

Zirconolite

The compositions of terrestrial and lunar zirconolites have been reviewed by Williams and Gieré (1996) who not only point out the wide range of elements which can substitute for Ca (e.g., the REE and actinides), but also highlight the large variations in the TiO_2 and ZrO_2 contents which can give rise to departures from the ideal formula of $CaZrTi_2O_7$. The composition of the zirconolite in BD3024 (Table 3, analyses 7–9) falls within the wide range of individual oxide contents listed by Williams and Gieré (1996), viz. CaO 1.83–16.54, ZrO_2 22.82–44.18, and TiO_2 13.56–44.91. CaO and TiO2 contents vary sympathetically, and both vary inversely with ZrO_2. In grains which show different brightnesses in BSE images, the brighter areas are high in Zr and contrast with darker high-CaTi areas. The zirconolite also contains appreciable FeO (3.85 wt%), together with significant Hf, Th, and Cr. Its REE values are unusual in that, although Ce and Nd are relatively high, Y, La and Pr contents are low. However, it may be noted that Ce is high compared with La in the parental zircon (Table 4, Fig. 7). Although not having the same high contents of Nb, Th and the REE as many carbonatite zirconolites, the BD3024 zirconolite has the low-Al, Fe > Mg and LREE > HREE characteristics considered by Gieré et al. (1998) to be specific to carbonatite zirconolites.

Compared with analyses listed by Williams and Gieré (1996), the BD3024 zirconolite is closest to that reported to be a reaction product in a zircon/ilmenite intergrowth in kimberlite from Kimberley, South Africa (Raber and Haggerty 1979; see Table 3, analysis 10). However, it is set apart from this intergrowth, and from zirconolites in other ultramafic parageneses (analyses 11 and 12) in containing no MgO or Al_2O_3. Most significantly, it is distinct from other terrestrial zirconolites in containing appreciable Cr_2O_3 (~0.8 wt%) which has only been reported in such concentrations in a very few lunar zirconolites.

Ilmenite

The ilmenite (Table 2, analysis 8) is a magnesian ilmenite-geikielite solid solution containing signficant Cr_2O_3 (1.11 wt%). Although the various oxide contents fall within the ranges reported for kimberlite megacryst or groundmass ilmenites, it differs in that stoichiometric calculations require no iron as Fe_2O_3. Like the diopside and phlogopite it is low in Al_2O_3, in this respect resembling MARID ilmenites. Contents of trace elements analysed at 25 spots on five different ilmenite grains are listed in Table 5. Elements occurring in significant amounts are Sc, V (though possibly enhanced by Mg molecular interference), Co, Zr, Hf, Nb, Ta and Pb. Although Sc, Co and Hf levels are reasonably constant, there are appreciable intragrain and intergrain variations in V (e.g., relatively low values in grain A2 compared with the other grains), Zr, Nb (e.g., range 1,400–2,400 ppm in grain A1), Ta and Pb. However, there are no systematic core/rim variations within the individual grains. Contents of La, Ce, Nd and Sm are very low and may well be spurious due to molecular Ti interference. W, Th and U values are mainly at the < 1-ppm level. The BD3024 ilmenite contents for Sc, Co and Hf fall within the ranges reported in kimberlite megacryst ilmenites (summarised by Mitchell 1986), whereas Zr, Nb and Ta contents are higher. It may be noted that

Table 4 Trace elements (ppm) in BD3024 and other mantle zircons. *S. Africa* Average of 56 zircons from on-craton South African kimberlites (Belousova et al. 1998). *Botswana* Average of seven "younger" kimberlite grains from the Jwaneng kimberlite, Botswana (Belousova et al. 1998). *Bultfontein*, *Monastery* Fragments of single zircon grains from kimberlite (Heaman et al. 1990). *MARID* Core and rim of zircon in MARID xenolith from Kamfersdam kimberlite, Kimberley, South Africa (Hamilton et al. 1998; D.G. Pearson, personal communication). Analysis annotation: *Letter* Polished section; *first number* Grain; *second number* Spot (thus, B3-3 is spot 3 on grain 3 in polished section 3024B)

Analysis	Sr	Y	Nb	Ba	La	Ce	Pr	Nd	Sm	Eu	Gd	Tb	Dy	Ho	Yb	Lu	Pb	Th	U	Th/U
A1-1	22.2	1,637.0	133.6	9.1	10.1	310.9	31.3	290.2	158.3	58.0	295.5	57.3	388.2	81.2	172.8	29.6	121.2	1,190	353.6	3.37
A1-2	24.0	1,520.0	113.4	12.0	10.3	263.6	26.0	240.1	132.8	49.5	262.7	51.1	360.9	77.9	174.8	29.6	178.9	994.3	331.1	3.00
A2-1	16.6	1,450.0	116.6	2.7	8.1	280.4	28.0	260.7	139.7	49.6	260.4	49.0	334.5	70.5	154.3	27.1	149.7	942.2	286.6	3.29
A2-2	17.1	1,249.0	96.0	3.0	5.5	212.1	20.7	197.0	114.4	39.6	218.1	41.5	284.7	59.6	130.7	22.2	154.2	768.0	221.7	3.46
A3-1	15.8	1,046.0	72.8	0.3	2.5	123.5	11.5	113.9	76.9	30.2	161.7	32.8	236.7	53.0	122.4	20.1	172.6	655.2	238.1	2.75
A3-2	14.6	1,267.0	98.4	0.0	5.1	201.8	19.3	195.2	115.5	43.2	223.7	44.0	309.1	64.8	145.3	24.4	163.0	848.0	260.2	3.26
A5-1	15.2	1,123.0	89.2	1.8	8.2	237.1	25.2	236	119	41.9	214.6	39.4	273.2	57.4	130.2	22.8	177.3	789.5	234.5	3.37
B1-1	26.2	1,664.0	123.0	13.8	12.0	325.2	34.8	311.5	166.6	62.0	299.0	57.1	402.8	85.7	200.4	32.2	188.2	1,142	374.4	3.05
B1-2	16.1	1,343.0	89.9	1.0	3.7	178.1	16.1	165.0	103.2	42.3	222.3	44.2	317.1	67.5	156.1	26.5	187.6	860.6	293.0	2.94
B1-3	16.3	1,459.0	311.8	0.8	11.0	346.8	34.9	322.2	160.1	56.3	283.6	52.0	353.2	72.3	157.0	25.7	199.4	2,203	629.3	3.50
B1-4	12.0	1,323.0	77.9	0.3	3.1	162.3	14.5	146.0	97.9	38.4	210.0	41.7	306.7	67.1	157.2	26.6	183.7	849.9	288.3	2.95
B1-5	11.3	1,558.0	125.3	11.0	8.8	264.6	25.5	241.6	136.2	49.7	254.4	49.7	359.7	78.9	183.4	30.3	178.9	1,005	347.5	2.89
B1-6	11.4	1,439.0	99.2	0.3	4.0	183.9	17.4	176.4	108.8	41.9	234.2	46.7	337.3	72.3	166.8	27.4	180.1	886.3	297.3	2.98
B2-2	12.1	6,44.4	198.5	46.2	4.4	120.3	9.8	90.9	53.6	20.1	107.8	21.5	147.8	32.2	72.1	11.7	203.4	1,346	438.2	3.07
B3-1	11.7	1,400.0	104.0	0.7	7.5	269.0	27.2	249.9	138.3	50.6	258.4	48.3	335.1	71.2	155.7	26.8	202.6	922.7	273.7	3.37
B3-2	11.9	1,750.0	121.9	4.6	11.1	329.8	35.3	315.5	168.3	59.8	304.6	58.4	419.5	87.7	200.1	32.9	170.5	1,248	389.9	3.20
B3-3	11.9	1,323.0	101.1	0.6	5.9	224.6	22.6	223.5	125.3	45.9	241.2	45.9	320.0	66.6	144.0	24.9	184.8	837.3	246.5	3.40
Avg	15.7	1,364.4	121.9	6.4	7.1	237.3	23.5	222.1	124.4	45.8	238.4	45.9	322.7	68.6	154.3	25.9	176.2	1,028.7	323.8	3.17
Std dev	4.6	262	57	11	3	70	8	69	31	11	50	9	65	13	31	5	21	354	99	0.23
S. Africa		45	3.4	0.4	0.1	1.2	0.1	0.7	0.9	0.5	2.4		5.8	1.6	7	1.3	1.3	4.6	12.8	0.36
Botswana		21	8.5	0.3	1.0	2.1	0.4	1.3	1.0	0.4	1.9		2.9	0.6	2.2	0.5	0.4	9.4	41.7	0.23
Bultfontein					2.5					1	0.89	1.3			8.6	2.2	0.4	7	23	0.30
Monastery											0.37	0.71			6.4	1.5	0.3	2	7	0.29
MARID core 1	14.3	303	10.6	0.25	0.35	18.8	0.86	9.77	9.28	3.26	19.2	5.88	49.8	12.8	54.5	10.9	185	86.2	71.2	1.21
MARID core 2	12.4	220	6.74	0.38	0.46	12.3	0.52	6.06	5.28	2.17	15.7	3.77	33.8	8.87	41.7	8.53	208	51.9	34.8	1.49
MARID rim 1	15.3	40.6	0.51	0.44	0.36	2.06	0.04	0.19	0.15	0.17	0.78	0.36	3.7	1.09	6.03	1.6	199	12	4.67	2.57
MARID rim 2	16.3	36.6	0.50	0.17	0.04	1.92	0.02	0.26	0.24	0.11	0.77	0.37	3.0	0.88	5.63	1.16	219	7.47	3.02	2.47

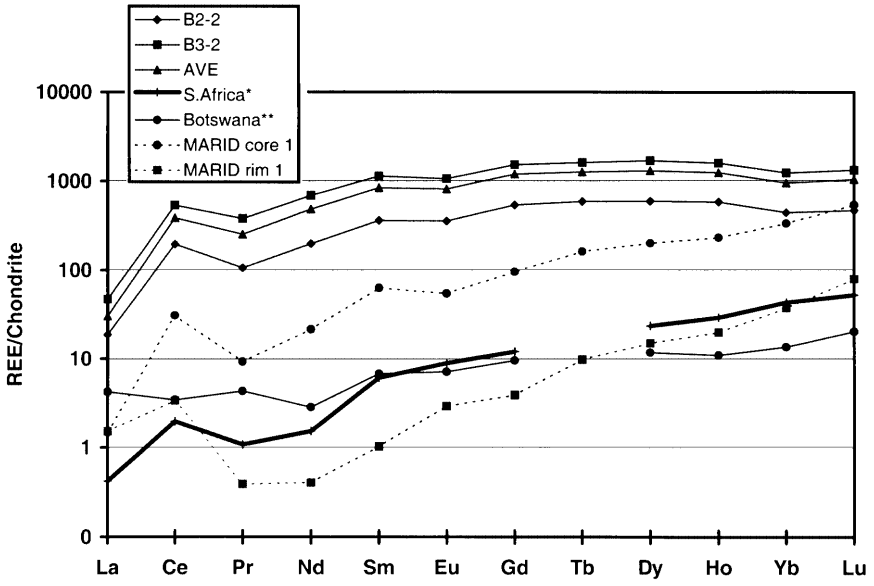

Fig. 7 REE plot of zircon from BD3024 and other mantle zircons (normalised against chondrite data of McDonough and Sun (1995); cf. Table 4). *B2-2* Highest values. *B3-2* Lowest values. *AVE* Average

the data summarised by Mitchell (1986) were produced by emission spectroscopy, neutron activation and XRF analysis of whole-megacryst samples. Comparative spot analyses for the above elements in kimberlite ilmenites are few, but electron-probe analyses have detected up to 1.53 wt% Nb_2O_5 and 0.61 wt% ZrO_2 in groundmass ilmenites in kimberlite dikes at Koidu, Sierra Leone (Tompkins and Haggerty 1985), up to 0.39% Nb_2O_5 and 0.08% ZrO_2 in ilmenite megacrysts from the Dalnaya kimberlite, Russia (Patchen et al. 1997), and 2.64% Nb_2O_5 in ilmenite from the Aries kimberlite, Australia (Edwards et al. 1992). Mitchell et al. (1973) have pointed out the enrichment in Zr in kimberlite ilmenites relative to other terrestrial ilmenites. The Zr contents in BD3024 ilmenites are even higher, although there is not a corresponding enhancement in Hf, as reflected in their higher Zr/Hf ratios (average 52.9) compared with kimberlite ilmenites (Zr/Hf 29–40).

Apatite

Apatite (Table 2, analysis 5) is a fluorapatite containing ~1 wt% LREE oxides. This is lower than the high contents often found in carbonatite apatites, and there is also an absence of SrO, the presence of which is held to be diagnostic of carbonatite apatites (Hogarth 1989). However, it does contain sufficient Na_2O (0.49 wt%) to make it similar to carbonatite apatites.

Calcite

The calcite (Table 2, analysis 4) is a low-Mg variety, the most distinctive feature of which is 0.31 wt% SrO. This can be matched in kimberlite calcites but is lower than that found in many carbonatite calcites (e.g., 0.45 to 2.68 wt%; Dawson et al. 1996).

Perovskite

The perovskite occurring in isolated grains contains slightly higher amounts of ZrO_2 and Nb_2O_5 than the perovskite replacing ilmenite, but the major-element contents (cf. Table 2, analyses 7 and 8) are so similar as to suggest that the groundmass grains derive from ilmenite reaction rims. Overall, the Zr, Fe, and Na contents can be matched in perovskites from kimberlites (Mitchell 1986), and the LREE, although present, are not as enriched as the levels generally recorded in perovskites from carbonatites and associated silicate rocks.

Spinel

The small (20 μm) spinel grain which occurs with perovskite in the reaction rims around ilmenite grains (Fig. 6) is a high-Ti magnetite which is unusual in containing substantial Cr_2O_3 (> 7 wt%) and significant NiO (0.48 wt%). The only comparable data from the literature is for a grain mantling corroded ilmenite in the Benfontein kimberlite, Kimberley (Boctor and Boyd 1981). The groundmass spinel differs from the reaction rim spinel (compare analyses 9 and 10, Table 2) in containing less Cr_2O_3 and MgO but higher Fe, and resembles the Ti-rich, Cr-poor end-members of a magmatic trend recognised in spinels from several kimberlite intrusions (see review by Mitchell 1986).

Heazlewoodite

Rare rounded 15–20-μm grains of heazlewoodite occur in the veins. A representative composition is Ni 70.9, Fe 1.53, Cu 0.17, S 26.7, total 99.30 wt%; structural formula $(Ni_{2.917}Fe_{0.066}Cu_{0.007})_{2.990}S_{2.009}$. Heazelwoodite is a comparatively rare mineral, having been reported mostly as a breakdown product of pentlandite in ser-

Table 5 BD3024 – Ilmenite trace element contents (ppm). Analysis annotation as in Table 4

Analysis	Sc	V[a]	Co	Y	Zr	Hf	Nb	Ta	La[b]	Ce[b]	Nd[b]	Sm[b]	W	Pb	Th	U	U	Zr/Hf	Nb/Ta
A1-1	36.9	851.8	229.7	0.29	1,491	29.9	1,434	215.0	0.31	0.42	0.59	2.06	0.12	21.1	0.01	0.01	0.01	49.8	6.7
A1-2	37.8	875.0	222.6	0.31	1,562	31.7	1,448	163.1	0.31	0.46	0.76	1.66	0.14	11.0	0.00	0.01	0.01	49.2	8.9
A1-3	38.3	949.6	225.9	0.29	1,673	33.8	2,444	252.8	0.35	0.56	0.86	3.07	0.14	50.9	0.01	0.02	0.02	49.6	9.7
A1-4	36.9	806.2	226.0	0.30	1,571	35.1	1,629	180.0	0.31	0.47	0.73	1.77	0.00	39.9	0.01	0.03	0.03	44.7	9.1
A1-5	39.1	884.7	233.0	0.33	1,657	36.8	1,805	204.3	0.27	0.51	0.67	2.50	0.21	25.9	0.00	0.01	0.01	45.0	8.8
A1-7	40.8	1,146.0	233.4	0.29	1,876	35.0	2,136	219.8	0.38	0.49	0.84	2.55	0.08	54.0	0.02	0.02	0.03	53.7	9.7
A2-1	36.9	766.1	269.3	0.30	1,399	27.6	2,119	218.4	0.36	0.42	0.85	2.00	0.30	72.9	0.01	0.03	0.02	50.8	9.7
A2-2	38.0	779.8	273.9	0.37	1,403	30.5	1,356	156.0	0.52	0.78	0.61	1.55	0.23	49.9	0.04	0.01	0.01	46.0	8.7
A2-3	36.7	835.4	272.4	0.27	1,448	28.0	1,881	192.5	0.34	0.43	0.60	2.23	0.00	43.3	0.03	0.04	0.04	51.7	9.8
C1-1	32.9	1,012.0	226.8	0.36	1,292	23.0	2,871	281.2	0.28	0.35	0.82	2.17	1.39	49.2	0.03	0.03	0.03	56.2	10.2
C1-2	30.0	925.1	225.3	0.38	1,221	23.3	5,438	974.5	0.47	0.61	1.48	6.22	3.15	47.9	0.02	0.06	0.06	52.4	5.6
C1-3	30.0	905.8	219.2	0.32	1,274	25.6	2,657	368.5	0.38	0.40	0.83	2.90	0.57	58.1	0.04	0.06	0.06	49.7	7.2
C1-4	30.8	995.7	227.0	0.36	1,248	22.0	4,058	520.4	0.39	0.52	1.33	4.89	1.91	75.3	0.04	0.04	0.04	56.8	7.8
C1-5	31.1	983.6	218.6	0.34	1,259	21.8	3,284	325.4	0.40	0.46	1.08	3.93	0.19	69.8	0.02	0.04	0.04	57.9	10.1
C1-6	30.9	846.9	213.7	0.44	1,365	24.2	2,316	271.4	0.34	0.43	0.62	3.02	0.30	89.9	0.02	0.02	0.02	56.5	8.5
C2-1	32.0	874.4	233.7	0.43	1,284	26.2	2,637	350.4	0.36	0.39	0.94	3.49	0.11	50.6	0.01	0.04	0.04	49.0	7.5
C2-2	32.7	860.4	243.5	0.34	1,376	26.2	2,525	315.8	0.42	0.55	1.11	3.22	0.50	71.5	0.09	0.05	0.05	52.5	8.0
C2-3	34.2	827.6	235.3	0.62	1,484	27.7	1,975	251.2	0.29	0.57	1.23	2.45	0.12	33.5	0.02	0.04	0.04	53.6	7.9
C2-4	33.0	856.4	234.2	0.39	1,340	25.6	1,484	174.5	0.32	0.43	0.63	1.84	0.25	58.9	0.02	0.03	0.03	52.4	8.5
C2-5	32.9	847.1	224.8	0.50	1,418	24.8	1,517	170.5	0.25	0.32	0.50	1.44	0.14	29.1	0.02	0.01	0.01	57.1	8.9
C2-6	32.2	887.1	232.2	0.40	1,299	20.0	3,443	281.7	0.34	0.46	1.02	3.72	0.33	102.1	0.01	0.07	0.07	64.9	12.2
C3-1	33.7	644.9	214.0	0.33	1,412	24.5	2,930	273.6	0.46	0.47	1.02	2.79	0.22	93.2	0.01	0.04	0.04	57.5	10.7
C3-2	30.4	706.7	194.4	0.39	1,279	22.4	3,318	281.9	0.35	0.50	0.73	4.23	0.29	57.2	0.00	0.03	0.03	57.0	11.8
C3-3	31.5	703.3	209.1	0.48	1,392	25.4	2,744	265.2	0.33	0.41	0.71	1.52	0.15	99.1	0.01	0.05	0.05	54.8	10.3
C3-4	30.3	689.6	204.5	0.38	1,251	22.8	2,112	229.3	0.31	0.38	0.52	1.66	0.19	73.9	0.01	0.04	0.04	54.8	9.2
Avg	34.0	858.45	229.7	0.37	1,411	27.0	2,462	285.5	0.35	0.47	0.84	2.75	0.46	57.1	0.02	0.03	0.03	52.9	8.6
SD	3.3	111.48	19.2	0.08	159	4.6	947	164.2	0.06	0.09	0.25	1.17	0.72	24.1	0.02	0.02	0.02	4.6	5.8
Kimberlite megacrysts[c]	19–80	1,000–2,000	139–366		385–1,269	15–32	477–1,521	47–174											

[a] 25Mg26Mg interference
[b] TiTiTi interference
[c] Extracted from Mitchell (1986)

pentinised orogenic peridotite complexes (Kullerud and Yund 1962). However, it has also been recorded in kimberlites as the result of olivine serpentinisation, and also a primary groundmass phase (see review by Mitchell 1986).

Discussion

Wall-rock metasomatism

Compared with the extensive and pervasive metasomatism occurring in some veined and metasomatised peridotite xenoliths from kimberlite, the metasomatic effects in specimen BD3024 are small, which is not unexpected alongside such thin veins. Metasomatism of the palaeosome olivine is restricted to rims adjacent to veins, where the olivine is altered to a higher Fe variety, comparatively enriched also in Mn and Ca. Similar enhancements have been reported in olivines in veined peridotites from Tanzania (Dawson and Smith 1988). However, the main effect has been the alteration of wall-rock enstatite to a mixture of diopside, richterite and phlogopite at its contact with the veins. This combination of new phases signals additions of Fe, Ti, Na, K, OH and F, but by far the most important effect is an increase in Ca to form diopside and richterite. As pointed out by Dawson (1987), a particular problem with Ca in many metasomatised peridotites is whether Ca is inherited and redistributed from pre-existing Ca-bearing phases (diopside and/or garnet), or introduced partly or wholly during metasomatism. In the specific case of BD3024, the absence of garnet and diopside in the palaeosome (though small amounts of Ca are present in the enstatite) means that the new Ca-bearing reaction minerals replacing wall-rock enstatite and changes in the Ca contents of the olivine rims adjacent to the veins can be largely attributed to Ca metasomatism. The veins themselves obviously hold high contents of Ca, as witnessed by the presence of diopside, zirconolite, perovskite apatite and calcite.

Zircon presence

Although zircon has been previously found in metasomatised peridotites and in MARID xenoliths (e.g., Gurney and Harte 1980; Haggerty and Gurney 1984; Konzett et al. 1998), it has not been identified in the two rare composite xenoliths which comprise MARID material in direct (? intrusive) contact with metasomatised peridotite (Waters et al. 1989; Boyd 1990). Hence, its identification in the vein paragenesis of composite xenolith BD3204 is worthy of note.

Zircon and ilmenite alteration

In BD3024, some zircons have been altered, and their initial replacement by ZrO_2 must have been due to a desilication reaction. Kresten et al. (1975), and Fiermans and Ottenburgs (1979), in describing kimberlite megacryst zircons which are coated with mixtures of monoclinic and tetragonal ZrO_2, attribute the coats to interaction between zircon and a carbonatitic liquid. Baddeleyite has also been found, together with zirconolite, diopside, sphene and calcite, at the interface between zircon and ilmenite in zircon/ilmenite intergrowths from one Lesothan and two South African kimberlites (Raber and Haggerty 1979). The formation of the interface assemblages in the subsolidus is suggested as having been triggered by a carbonatitic fluid which provided the necessary Ca to form diopside and zirconolite. It would appear intuitively that a high-Ca/low-Si environment is favourable for baddeleyite formation. Certainly baddeleyite is the usual Zr phase in carbonatite complexes (e.g., Phalaborwa), and baddeleyite, calzirtite and an unnamed Ca-Zr oxide have been found as primary phases (Scatena-Wachel and Jones 1984; Mitchell 1994) in the kimberlite of the Benfontein sills which is sufficiently high in calcite to have been referred to as carbonatitic (Dawson and Hawthorne 1973).

In BD3024, there is textural evidence for (1) peripheral replacement of zircon by baddeleyite, and (2) replacement of baddeleyite by zirconolite (addition of Ca and Ti). These are very localised reactions, and not all zircon grains are similarly affected. Although there is direct contact between zircon and zirconolite in some composites, textural evidence for replacement of zircon by zirconolite is ambiguous; and it appears more likely that zirconolite has completely replaced the baddeleyite which formerly rimmed zircon. Further, the formation of zirconolite around zircons not in contact with, or in the immediate vicinity of ilmenite grains indicates that, as proposed in the Raber and Haggerty (1979) model, ilmenite-zircon interaction (with the involvement of carbonatitic Ca) is not the case for BD3024 zirconolite. A more simple explanation is that the zirconolite formed by interaction of baddeleyite with the same Ca- and Ti-rich fluids which subsequently precipitated ilmenite, and that the later ilmenite grains sometimes partially enclosed the zircon-baddeleyite-zirconolite composites. Hence, the suggested reactions are

$$\underset{ZrSiO_4}{\text{Zircon(minus } SiO_2)} \rightarrow \underset{ZrO_22}{\text{Baddeleyite(plus Ca and Ti)}} \rightarrow \underset{CaZrTi_2O_7}{\text{Zirconolite}}$$

The zircon was an early precipitate from the liquid which precipitated the other vein phases and, at that stage, the magma must have been sufficiently saturated in SiO_2 to precipitate zircon rather than ZrO_2. A change in the magma chemistry must have occurred, with the magma first having reduced the silica content (resulting in baddeleyite), subsequently becoming enhanced in Ca and Ti, and reacting with the baddeleyite to form zirconolite. Similarly, ilmenite reacted with a Ca-rich fluid to form perovskite rims.

As to the nature of the magma, the coincidence of the date recorded for the zircon grains with the age of the Kimberley area kimberlite magmatism (Kinny and

Dawson 1992) suggests kimberlite as a possible candidate, a possibility supported by the high-K, Ti, Mg, Ca, and OH nature of the magma, inferred from the mineralogy of the veins.

However, inversion of the REE data for the BD3024 average zircon, using the zircon/liquid partitioning data of Hinton and Upton (1991), indicates that the zircon must have been in equilibrium with a magma which was highly enriched in the LREE (La 3,600 × chondrite), with a very steep slope towards low HREE contents (La/Lu_{CN} ratio ~1,600, i.e. > three orders of magnitude). Kimberlites, both group I and group II (orangeites), although having LREE enhancement and steeply sloping patterns (summarised by Mitchell 1986, s1995), contain lower amounts of all the REE than this calculated magma. The only magmatic rocks which consistently match these calculated parameters are carbonatites (e.g., see Woolley and Kempe 1989). However, carbonate is rare in the veins which (if the veins formed from a carbonatitic melt) implies that they are the result of open-system crystallisation, and that the vein phases are the early precipitates plating the vein walls. The lost liquid residue of this magma must have had a very low viscosity to enable it to migrate onwards before the freezing of the very thin veins. This again points to carbonatite, as currently it is the only magma type known to possess such very low viscosities (Treiman 1989).

In the case of the alteration rims around ilmenite (Fig. 6), as in the case of the zirconolite rims on zircon, there must have been interaction with a Ca-rich medium to produce the perovskite. Nonetheless, although crystallisation from REE-enriched melt appears to be valid for zircon, later crystallising phases such as zirconolite, apatite, calcite and perovskite do not have the same REE contents as their analogues in carbonatites.

A simple model might be that a calcite-rich kimberlite intruded minor fractures in the harzburgite palaeosome, inter alia causing Ca metasomatism of the palaeosome. After initial precipitation of diopside, zircon, phlogopite and ilmenite, most of the residual liquid migrated, though interstitial serpentine, calcite and apatite may represent small amounts of nonmigrated residual liquid. Such a model, drawing in part on the zircon and ilmenite alteration, implies evolution and substantial changes in the magma chemistry during cooling. In this context, it is pertinent to note that pre-emplacement changes in kimberlite magma chemistry have been previously reported from the Kimberley area in the fractionated carbonate-rich kimberlite of the Benfontein sills (Dawson and Hawthorne 1973).

Acknowledgements Paula McDade and John Craven are thanked for their help with the analytical work, and the polished sections were prepared by Mike Hall. Richard Hinton and Steve Haggerty gave useful advice on zircon-liquid partitioning and oxide mineralogy, respectively. Helpful reviews were provided by Steve Haggerty and Terry Williams. We are also grateful to Graham Pearson for providing prepublication data on his MARID zircon. The electron- and ion-probe facilities at the University of Edinburgh are supported by N.E.R.C.

References

Allsopp HL, Barrett DR (1975) Rb-Sr age determinations on South African kimberlite pipes. Phys Chem Earth 9:605–617

Bailey DK (1982) Mantle metasomatism – continuing chemical change within the Earth. Nature 296:525–530

Bailey DK, Lloyd FE (1975) Light element metasomatism of the continental mantle: the evidence and the consequences. Phys Chem Earth 9:389–416

Belousova EA, Griffin WL, Pearson NJ (1998) Trace element composition and cathodoluminescence properties of southern African kimberlitic zircons. Mineral Mag 62:355–366

Boctor NZ, Boyd FR (1981) Oxide minerals in a layered kimberlite-carbonate sill from Benfontein, South Africa. Contrib Mineral Petrol 76:253–259

Boyd FR (1990) Mantle metasomatism: evidence from a MARID-harzburgite compound xenolith. Carnegie Inst Washington Yearb 90:18–23

Boyd FR, Pearson DG, Nixon PH, Mertzman SA (1993) Low-calcium garnet harzburgites from southern Africa: their relation to craton structures and diamond crystallisation. Contrib Mineral Petrol 113:352–366

Carswell DA (1975). Primary and secondary phlogopites and clinopyroxenes in garnet lherzolite xenoliths. Phys Chem Earth 9:417–429

Dawson JB (1984) Contrasting types of mantle metasomatism? In: Kornprobst J (ed) Kimberlites II: The mantle and crust-mantle relationships. Elsevier, Amsterdam, pp 289–294

Dawson JB (1987) Metsomatised harzburgites in kimberlite and alkaline magmas: enriched restites and ''flushed'' lherzolites. In: Menzies MA, Hawkesworth CJ (eds) Mantle metasomatism. Academic Press, London, pp 125–144

Dawson JB (1999) Melting and metasomatism in spinel peridotite xenoliths from Labait, Tanzania. In: Gurney JJ, Gurney JL, Pascoe MD, Richardson SH (eds) Proc 7th Int Kimberlite Conf. Red Roof Design, Cape Town, pp 164–173

Dawson JB, Hawthorne JB (1973) Magmatic sedimentation and carbonatitic differentiation in kimberlite sills at Benfontein, South Africa. J Geol Soc Lond 129:113–131

Dawson JB, Hill PG (1998) Mineral chemistry of a peralkaline combeite lamprophyllite nephelinite from Oldoinyo Lengai, Tanzania. Mineral Mag 62:179–196

Dawson JB, Smith JV (1975) Chromite-silicate intergrowths in upper-mantle peridotites. Phys Chem Earth 9:339–350

Dawson JB, Smith JV (1977) The MARID (mica-amphibole-rutile-ilmenite-diopside) suite of xenoliths in kimberlite. Geochim Cosmochim Acta 41:309–323

Dawson JB, Smith JV (1988) Metasomatised and veined upper mantle xenoliths from Pello Hill, Tanzania: evidence for anomalously-light mantle beneath the Tanzanian sector of the East African Rift Valley. Contrib Mineral Petrol 100:510–527

Dawson JB, Smith JV, Hervig RL (1977) Late-stage diopside in kimberlite groundmass. Neues Jahrb Mineral Monatsh 1977:529–543

Dawson JB, Smith JV, Hervig RL (1980) Heterogeneity in upper-mantle lherzolites and harzburgites. Philos Trans Roy Soc Lond A297:323–331

Dawson JB, Steele IM, Smith JV, Rivers ML (1996) Minor and trace element chemistry of carbonates, apatites and magnetites in some African carbonatites. Mineral Mag 60:415–425

Delaney JS, Smith JV, Carswell DA, Dawson JB (1980) Chemistry of micas from kimberlites and xenoliths – II. Primary- and secondary-textured micas from peridotite xenoliths. Geochim Cosmochim Acta 44:842–857

Edwards D, Rock NMS, Taylor WR, Griffin BJ, Ramsay RR (1992) Mineralogy and petrology of the Aries diamondiferous kimberlite pipe, Central Kimberley Block, Western Australia. J Petrol 33:1157–1191

Erlank AJ, Waters FG, Hawkesworth CJ, Haggerty SE, Allsopp HL, Rickard RS, Menzies MA (1987) Evidence for mantle metasomatism in peridotite nodules from the Kimberley pipes,

South Africa. In: Menzies MA, Hawkesworth CJ (eds) Mantle metasomatism. Academic Press, London, pp 125–144
Fieremans M, Ottenburgs R (1979) The occurrence of zircon and baddeleyite crystals in the kimberlite formations at Mbuji-Mayi (Bakwanga, Zaire). Bull Soc Belg Géol 88:25–31
Fowler M, Williams CT (1986) Zirconolite from the Gen Dessary syenite: a comparison with other Scottish localities. Mineral Mag 50:326–328
Gieré R, Williams CT, Lumpkin GR (1998) Chemical characteristics of natural zirconolite. Schweiz Mineral Petrogr Mitteil 78:433–459
Gurney JJ, Harte B (1980) Chemical variations in upper mantle nodules from southern Africa. Phil Trans Roy Soc Lond A297:273–293
Haggerty SE, Gurney JJ (1984) Zircon-bearing nodules from the upper mantle. EOS 65:305
Haggerty SE, Smyth JR, Erlank AJ, Rickard RS, Danchin RV (1983) Lindsleyite (Ba) and mathiasite (K): two new chromium-titanates in the crichtonite series from the upper mantle. Am Mineral 68:494–505
Haggerty SE, Grey IE, Madsen IC, Criddle AJ, Stanley CJ, Erlank AJ (1989) Hawthorneite, $Ba[Ti_3Cr_4Fe_4Mg]O_{19}$: A new metasomatic magnetoplumbite-type mineral from the upper mantle. Am Mineral 74:668–675
Hamilton MA, Pearson DG, Stern RA, Boyd FR (1998) Constraints on MARID petrogenesis: SHRIMP II U-Pb zircon evidence for pre-eruption metasomatism at Kamfersdam. 7th Int Kimberlite Conf, Cape Town. Extend Abstr Vol, pp 296–298
Harte B, Winterburn PA, Gurney JJ (1987) Metasomatic and enrichment phenomena in garnet peridotite facies mantle xenoliths from the Matsoku kimberlite pipe, Lesotho. In: Menzies MA, Hawkesworth CJ (eds) Mantle metasomatism. Academic Press, London, pp 145–220
Heaman LM, Le Cheminant AN (1993) Paragenesis and U-Pb systematics of baddeleyite (ZrO_2). Chem Geol 110:95–126
Heaman LM, Bowins R, Crocket J (1990) The chemical composition of igneous rock suites: implications for geochemical tracer studies. Geochim Cosmochim Acta 54:1597–1607
Hervig RL, Smith JV, Steele IM, Dawson JB (1980) Fertile and barren Al-Cr-spinel harzburgites from the upper mantle: ion and electron-probe analyses of trace elements in olivine and orthopyroxene: relation to lherzolites. Earth Planet Sci Lett 50:41–58
Hervig RL, Smith JV, Dawson JB (1986) Lherzolite xenoliths in kimberlites and basalts: petrogenetic and crystallochemical significance of some minor and trace elements in olivines, pyroxenes, garnet and spinel. Trans Roy Soc Edinburgh, Earth Sci 77:181–201
Hinton RW, Upton BGJ (1991) The chemistry of zircon: variations in and between large crystals from syenite and alkali basalt xenoliths. Geochim Cosmochim Acta 55:3287–3302
Hogarth DD (1989) Pyrochlore, apatite and amphibole: distinctive minerals in carbonatite. In: Bell K (ed) Carbonatites. Unwin Hyman, London, pp 105–148
Hoskin PWO, Ireland TR (2000) Rare earth element chemistry of zircon and its use as a provenance indicator. Geology 28: 627–630
Jones AP, Smith JV, Dawson JB (1982) Mantle metasomatism in 14 veined peridotites from Bultfontein Mine, South Africa. J Geol 90:435–443
Kinny PD, Dawson JB (1992) A mantle metasomatic injection event linked to late Cretaceous kimberlite magmatism. Nature 360:726–728
Kinny PD, Meyer HOA (1994) Zircon from the mantle: a new way to date old diamonds. J Geol 102:475–481
Konzett J, Armstrong RA, Sweeney RJ, Compston W (1998) The timing of MARID metasomatism in the Kaapvaal mantle: an ion probe study of zircons from MARID xenoliths. Earth Planet Sci Lett 160:133–145
Kramers JD, Roddick JC, Dawson JB (1983) Trace element and isotope studies on veined, metasomatic and MARID xenoliths from Bultfontein, South Africa. Earth Planet Sci Lett 65:90–106
Kresten P, Fels P, Berggren G (1975) Kimberlitic zircons – a possible aid in prospecting for kimberlites. Mineral Deposita 10:47–56
Kullerud G, Yund RA (1962) The Ni-S system and related minerals. J Petrol 3:126–175
Lorand JP, Cottin JY (1987) A new natural occurrence of zirconolite ($CaZrTi_2O_7$) and baddeleyite (ZrO_2) in basic cumulates: the Laouni layered intrusion (Southern Hoggar). Mineral Mag 51:671–676
McDonough WF, Sun SS (1995) The composition of the Earth. Chem Geol 120:223–253
Menzies MA, Hawkesworth CJ (eds) (1987) Mantle metasomatism. Academic Press, London
Mitchell RH (1986) Kimberlites. Plenum Press, New York
Mitchell RH (1994) Accessory rare earth, strontium, barium and zirconium minerals in the Benfontein and Wesselton calcite kimberlites, South Africa. In: Meyer HOA, Leonardos OH (eds) Kimberlites, related rocks and xenoliths, Vol 1. Proc 5th Int Kimberlite Conf, Araxa, Brazil. Companhia de Pesquisa de Recursos Minerais, Rio de Janeiro, pp 115–128
Mitchell RH (1995) Kimberlites, orangeites and related rocks. Plenum Press, New York
Mitchell RH, Brunfelt AO, Nixon PH (1973) Trace elements in magnesian ilmenites from Lesotho kimberlites. In: Nixon PH (ed) Lesotho kimberlites. Lesotho Nat Dev Corp, Maseru, pp 230–235
Navon O, Stolper E (1987) Geochemical consequences of melt percolation: The upper mantle as a chromatographic column. J Geol 95:285–307
Patchen AD, Taylor LA, Pokhilenko N (1997) Ferrous freudenbergite in ilmenite megacrysts: a unique paragenesis from the Dalnaya kimberlite, Yakutia. Am Mineral 82:991–1000
Raber E, Haggerty SE (1979) Zircon-oxide reactions in diamond-bearing kimberlites. In: Boyd FR, Meyer HOA (eds) Kimberlites, diatremes and diamonds: their geology, petrology and geochemistry. Am Geophys Union, Washington, DC, pp 229–240
Scatena-Wachel DE, Jones AP (1984) Primary baddeleyite (ZrO_2) in kimberlite from Benfontein, South Africa. Mineral Mag 48:257–261
Schärer U, Corfu F, Demaiffe D (1997) U-Pb and Lu-Hf isotopes in baddeleyite and zircon megacrysts from the Mbuji-Mayi kimberlite: constraints on the subcontinental mantle. Chem Geol 143:1–16
Smith JV, Dawson JB (1975) Chemistry of Ti-poor spinels, ilmenites and rutiles from peridotite and eclogite xenoliths. Phys Chem Earth 9:309–322
Smith JV, Brennesholtz R, Dawson JB (1978) Chemistry of micas from kimberlites and xenoliths – I. Micaceous kimberlites. Geochim Cosmochim Acta 42:959–971
Stephens WE, Dawson JB (1977) Statistical comparison between pyroxenes from kimberlites and their associated xenoliths. J Geol 85:433–449
Tompkins LA, Haggerty SE (1985) Groundmass oxides in the Koidu kimberlite dikes, Sierra Leone, West Africa. Contrib Mineral Petrol 91:245–263
Treiman AH (1989) Carbonatite magma: properties and processes. In: Bell K (ed) Carbonatites. Unwin Hyman, London, pp 89–104
Waters FG (1987) A suggested origin of MARID xenoliths in kimberltes by high pressure crystallisation of an ultrapotassic rock such as lamproite. Contrib Mineral Petrol 95:523–533
Waters FG, Erlank AJ, Daniels LRM (1989) Contact relationships between MARID rock and metasomatised peridotite in a kimberlite xenolith. Geochem J 23:11–17
Williams CT, Gieré R (1996) Zirconolite: a review of localities worldwide, and a compilation of its chemical compositions. Bull Nat Hist Mus Lond (Geol) 52:1–24
Wilshire HG, Pike JEN, Meyer CE, Schwarzman EC (1980) Amphibole-rich veins in lherzolite xenoliths, Dish Hill and Deadman Lake, California. Am J Sci 280-A:576–593
Woolley AR, Kempe DRC (1989) Carbonatites: nomenclature, average chemical composition and element distribution. In: Bell K (ed) Carbonatites. Unwin Hyman, London, pp 1–14
Zinner E, Crozaz G (1986) A method for the quantitative measurement of rare earth elements in the ion microprobe. Int J Mass Spectrom Ion Proc 69:17–38